Soil Dynamics & Earthquake Engineering (Vol. 27, No. 1, pp. 14-28, 2007)

On the influence of the polarization and the shape of the strain loop on strain accumulation in sand under high-cyclic loading

T. Wichtmann[i)], A. Niemunis, Th. Triantafyllidis

Institute of Soil Mechanics and Foundation Engineering, Ruhr-University Bochum, Universitätsstraße 150, 44801 Bochum, Germany

Abstract

This paper presents results of cyclic triaxial tests on sand with a simultaneous variation of the axial and the lateral stresses. Furthermore, a cyclic multidimensional simple shear (CMDSS) device and corresponding test results are discussed. For in-phase cycles with a constant strain amplitude it is demonstrated that the accumulation rate is independent of the polarization of the cycles in the strain space. Polarization changes lead to a temporary increase of the accumulation rate: they increase the effectiveness of compaction. For out-of-phase (e.g. elliptical) cycles the shape of the strain loop significantly influences the residual strain. A circular strain loop generates twice larger accumulation rates than a one-dimensional strain loop with identical span. The accumulation rate is not influenced by the circulation of the strain loop. It is shown that the direction of accumulation (so-called "cyclic flow rule") is only moderately affected by the polarization and the shape of the cycles.

Key words: Cyclic triaxial tests; Cyclic multidimensional simple shear tests; In-phase cycles; Out-of-phase cycles; Strain accumulation; Sand

1 Introduction

The cyclic stress and strain paths in the soil can be *in-phase* or *out-of-phase*. The in-phase (one-dimensional) loops are usually caused by quasi-static fixed sources like watergates, tanks, etc. In the case of traffic loads, a passing wheel (Fig. 1) for example, the stress and strain loops are out-of-phase, i.e. they encompass some stress or strain space. Moreover, a rotation of the principal stress axes in the soil takes place. The most prominent example of out-of-phase loops are the ubiquitous Rayleigh waves. They cause elliptical strain loops. Rayleigh waves carry about 90 % of the vibration energy and are therefore practically the most important types of wave. The second author has already shown [1] that the popular estimation of the amplitude $\gamma^{\text{ampl}} = \dot{u}/v_S$ for shear waves with the material point velocity $\dot{u}$ in the vertical direction and the shear wave velocity v_S does not apply to Rayleigh waves. Our present tests demonstrate furthermore that out-of-phase loops produce larger accumulation rates than in-phase cycles. Thus, ignoring the out-of-phase nature of the cycles can under-estimate the residual deformations or the pore pressure generation. In most studies on the development of permanent deformations under cyclic loading, cyclic simple shear tests or cyclic triaxial tests with a constant lateral stress σ_3 were performed in which out-of-phase loops were not examined.

The *polarization* describes the orientation of the loop in the stress/strain space. A more general definition is given in [2, 3]. It is worth to take a closer look on the influence of the polarization of the cycles on the accumulation of permanent deformations. Only few experimental studies dealing with this topic can be found in the literature. In-phase cycles may change their polarization in situ, e.g. in the case of a stochastic cyclic loading due to wind and waves (e.g. coastal structures, wind power plants on- and offshore). The effect of a change of the polarization on the accumulation of deformations in the soil is not well-understood yet. Our test results show that such polarization changes lead to an increased accumulation rate. They demonstrate furthermore that the effectiveness of soil compaction can

[i)] Corresponding author. Tel.: + 49-234-3226080; fax: +49-234-3214150; *e-mail address:* torsten.wichtmann@rub.de

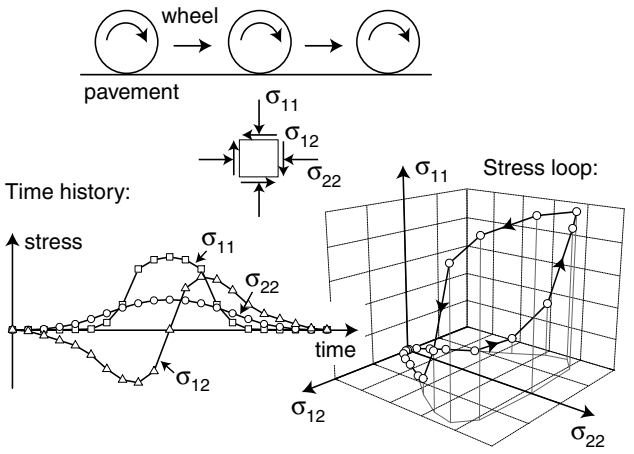

Fig. 1: Out-of-phase stress loops in the soil due to traffic loads on the surface

be enhanced by a suitable variation of the polarization.

The aim of our research is the development of a method for the prediction of permanent deformations in the soil under cyclic (quasi-static or dynamic) loading with a large number of cycles ($N > 10^4$) and small amplitudes ($\varepsilon^{\mathrm{ampl}} < 10^{-3}$, so-called high-cyclic loading). An explicit accumulation model [3] for sand has been developed for this purpose. It is briefly summarized in Section 4. The model is based on results of tests with $\sigma_3 =$ constant which are documented in [4] (tests with triaxial compression) and [5] (tests with triaxial extension). The influence of the strain amplitude, the average stress, the void ratio and the cyclic preloading on the accumulation rate was implemented into the model.

An explicit model should describe the accumulation due to in-phase *and* out-of-phase strain loops, the influence of the polarization of the cycles and the effect of polarization changes. Unfortunately, apart from the model proposed by the authors, none of the explicit models in the literature (a survey is given in [6]) considers these demands. They commonly use the shear strain amplitude γ^{ampl}, which is defined for in-phase cycles and which ignores the volumetric portion of the strain loop. Polarization effects are usually not captured either.

The formulation of an explicit model requires high-quality cyclic test data. Unfortunately, only few experimental works deal with the effect of the shape and the polarization of the stress or strain cycles on the rate of strain accumulation. The tests in the literature are usually restricted to very few cycles ($N < 100$) most of which are performed under undrained conditions. A survey of the literature is given in Section 3.

We have performed much more laborious drained tests on sand with large numbers of cycles. In cyclic triaxial tests $\sigma_1(t)$ and $\sigma_3(t)$ have been cyclically varied *with* (out-of-phase cycles) and *without* (in-phase cycles) a phase-shift in time. The influence of the shape of the cycles was also tested in a cyclic multidimensional simple shear (CMDSS) device. This novel apparatus was further used for studies of the influence of the circulation and polarization changes.

2 Notation and definitions

The sign convention of soil mechanics (compression positive) is used. The Roscoe invariants p (mean pressure) and q (deviatoric stress) of the Cauchy stress $\boldsymbol{\sigma}$ are

$$p = \mathrm{tr}\,\boldsymbol{\sigma}/3 \overset{\mathrm{triax}}{=} (\sigma_1 + 2\,\sigma_3)/3 \qquad (1)$$

$$q = \sqrt{3/2}\;\|\boldsymbol{\sigma}^*\| \overset{\mathrm{triax}}{=} \sigma_1 - \sigma_3 \qquad (2)$$

with $\|\sqcup\|$ denoting the Euclidian norm and $\sqcup^*$ giving the deviatoric portion of $\sqcup$. In the axially symmetric triaxial test $\sqcup_1$ denotes the axial component and $\sqcup_3$ the lateral component of stress or strain, respectively. Alternatively, we use the isomorphic variables $P = \sqrt{3}\;p$ and $Q = \sqrt{2/3}\;q$ [2]. With isomorphic variables, two vectors which are orthogonal to each other in the three-dimensional σ_1-σ_2-σ_3-principal stress system are also perpendicular to each other in the P-Q-plane. Furthermore, they preserve their lengths. This does not apply to the p-q-coordinate system [2]. The stress obliquity is $\eta = q/p$ (Fig. 2). It takes the values $M_c = (6\,\sin\varphi)/(3 - \sin\varphi)$ for compression and $M_e = -(6\,\sin\varphi)/(3 + \sin\varphi)$ for extension with the critical friction angle $\varphi = \varphi_c$ for the critical state line (CSL) and the peak friction angle $\varphi = \varphi_p$ for the maximum shear strength. Figure 2 shows typical IP and OOP stress paths of the cyclic triaxial tests in which the average stress $\boldsymbol{\sigma}^{\mathrm{av}}$ is superposed by a linear and an elliptical cyclic portion, respectively.

It is distinguished between *in-phase (IP)* and *out-of-phase (OOP)* - cycles. In the following the meaning of IP and OOP is explained for the triaxial case (Fig. 3). In the case of IP-cycles all components of $\boldsymbol{\sigma}$ oscillate "in phase", i.e. with the same scalar, periodical function $-1 \le f(t) \le 1$ in time t (e.g. $f(t) = \sin(t)$), i.e. $\boldsymbol{\sigma} = \boldsymbol{\sigma}^{\mathrm{av}} + \boldsymbol{\sigma}^{\mathrm{ampl}} f(t)$. A special case of the IP-cycles are the *uniaxial* cycles (Fig. 3a), where only one component varies with time, e.g.:

$$\boldsymbol{\sigma} = \boldsymbol{\sigma}^{\mathrm{av}} + \mathrm{diag}\left(\sigma_1^{\mathrm{ampl}}, 0, 0\right)\; f(t) \qquad (3)$$

In all other cases the IP-cycles are *multiaxial* (Fig. 3b):

$$\boldsymbol{\sigma} = \boldsymbol{\sigma}^{\mathrm{av}} + \mathrm{diag}\left(\sigma_1^{\mathrm{ampl}}, \sigma_3^{\mathrm{ampl}}, \sigma_3^{\mathrm{ampl}}\right)\; f(t) \qquad (4)$$

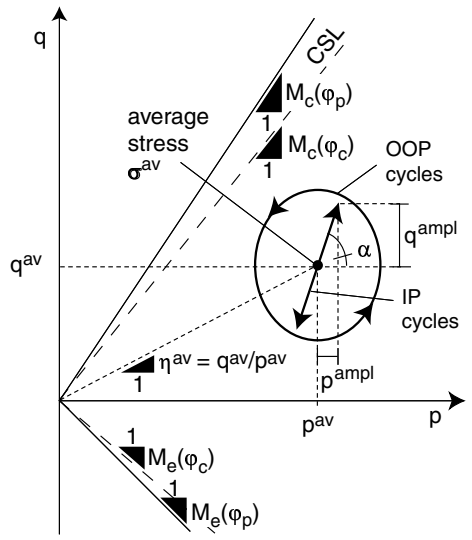

Fig. 2: Cyclic stress path in the p-q-plane

In OOP-cycles (Fig. 3c) the components may oscillate with a phase shift θ, e.g.:

$$\boldsymbol{\sigma} = \boldsymbol{\sigma}^{\mathrm{av}} + \mathrm{diag}\left(\sigma_1^{\mathrm{ampl}}\ f(t), \sigma_3^{\mathrm{ampl}}\ f(t+\theta), \sigma_3^{\mathrm{ampl}}\ f(t+\theta)\right) \quad (5)$$

In the cyclic triaxial test with σ_3 = constant uniaxial IP-stress cycles are applied. If $\sigma_3 \neq$ constant and σ_1 and σ_3 oscillate without a phase shift multiaxial IP-stress cycles are obtained. An oscillation *with* a phase shift θ results in OOP-cycles.

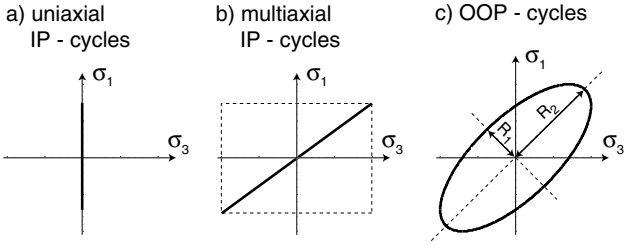

Fig. 3: Distinction between uniaxial IP-, multiaxial IP- and OOP-cycles

We denote the strain $\boldsymbol{\varepsilon}$ and use the strain invariants

$$\varepsilon_v = \mathrm{tr}\,\boldsymbol{\varepsilon} \overset{\mathrm{triax}}{=} \varepsilon_1 + 2\,\varepsilon_3 \quad (6)$$

$$\varepsilon_q = \sqrt{2/3}\ \|\boldsymbol{\varepsilon}^*\| \overset{\mathrm{triax}}{=} 2/3\ (\varepsilon_1 - \varepsilon_3) \quad (7)$$

(ε_v: volumetric strain, ε_q: deviatoric strain). The norm of the strain is

$$\varepsilon = \|\boldsymbol{\varepsilon}\| \overset{\mathrm{triax}}{=} \sqrt{(\varepsilon_1)^2 + 2(\varepsilon_3)^2} = \sqrt{(\varepsilon_P)^2 + (\varepsilon_Q)^2}. \quad (8)$$

The isomorphic strain invariants are $\varepsilon_P = 1/\sqrt{3}\ \varepsilon_v$ and $\varepsilon_Q = \sqrt{3/2}\ \varepsilon_q$. In the case of cyclic loading the strain $\boldsymbol{\varepsilon}$ is composed of an accumulated (residual) portion $\boldsymbol{\varepsilon}^{\mathrm{acc}}$ and an elastic (resilient) portion $\boldsymbol{\varepsilon}^{\mathrm{ampl}}$. The accumulation rate is $\dot{\boldsymbol{\varepsilon}}^{\mathrm{acc}} = \partial\boldsymbol{\varepsilon}^{\mathrm{acc}}/\partial N$, i.e. in this context the superposed dot means a derivative with respect to the number of cycles N. The ratio $\omega = \varepsilon_v^{\mathrm{acc}}/\varepsilon_q^{\mathrm{acc}}$ is used for the direction of accumulation. In general, the so-called "cyclic flow rule" is a tensor $\mathbf{m} = \dot{\boldsymbol{\varepsilon}}^{\mathrm{acc}}/\|\dot{\boldsymbol{\varepsilon}}^{\mathrm{acc}}\|$. The density is described by the index $I_D = (e_{\max} - e)/(e_{\max} - e_{\min})$ with void ratio e ($I_D = D_r\ \varrho_{d,\max}/\varrho_d$ with relative density D_r and dry density ϱ_d). The initial value after consolidation prior to cyclic loading is denoted by I_{D0}.

3 Survey of literature

For tests with σ_3 = constant please see a literature survey in [4].

3.1 Influence of the polarization of the cycles

The influence of the polarization was rarely studied in the past. Mostly a pure deviatoric shearing in the simple shear test or predominant deviatoric cycles in the triaxial test with σ_3 = constant were investigated. Ko & Scott [7] studied the effect of repeated cycles with hydrostatic compression on the accumulation of strains in cubical specimens. The tests showed a small compression of the specimens during the first cycles whereas no strain accumulation was observed during the following cycles. The tests of Ko & Scott [7] were restricted to very few cycles.

Choi & Arduino [8] performed undrained true triaxial tests on cubical specimens of gravel. At an initial isotropic effective pressure stress cycles with an identical amplitude but with different polarizations in the deviatoric plane were tested. No dependence of the liquefaction resistance on the polarization of the cycles could be detected.

3.2 Influence of polarization changes

Yamada & Ishihara [9] studied the influence of a change of the polarization in drained tests on loose saturated sand in true triaxial tests. After isotropic consolidation four cycles were tested. In the first cycle a certain octahedral shear stress amplitude ($\tau_{\mathrm{oct}} = (\boldsymbol{\sigma}^* : \boldsymbol{\sigma}^*)/\sqrt{3}$) was applied at p = constant (Fig. 4). In the second cycle the loading was rotated by the angle θ in the octahedral plane keeping the amplitude constant. The third cycle was applied in the same direction as the first cycle, but the amplitude was increased. In the fourth cycle the specimen was sheared again in the direction of the second cycle with the same amplitude as in the third cycle. Yamada & Ishihara observed (Fig. 4), that

the residual strain after the second and the fourth cycle increased with θ, i.e. with increasing rotation of the shearing direction in the second and the fourth cycle with respect to the polarization in the first and the third cycle. They concluded, that the material "forgets" (at least partly) its loading history, if the actual direction of loading deflects from the previous polarization.

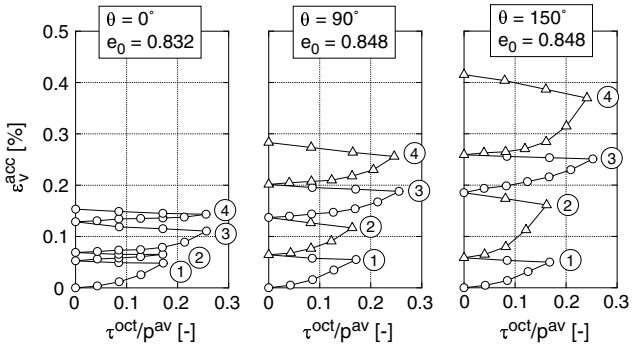

Fig. 4: True triaxial tests after Yamada & Ishihara [9]: Influence of a rotation of the stress path by $\theta = 0°$, 90° and 150° on the accumulation of volumetric strain

3.3 Influence of the shape of the cycles

Pyke et al. [10] tested dry sand under multiaxial cyclic loading. Two shaking tables were used. One was mounted transversely on the other one allowing for 2-D shearing. If the applied stress path was approximately circular the settlement was twice larger than for an uniaxial stress path with the same maximum shear stress (Fig. 5). Furthermore, if two stochastically generated loadings $\tau_1(t)$ and $\tau_2(t)$ with $\tau_1^{\mathrm{ampl}} \approx \tau_2^{\mathrm{ampl}}$ were applied simultaneously, the resulting settlement was twice larger than in the case where the sand layer was sheared only with $\tau_1(t)$ or only with $\tau_2(t)$. It was concluded that if sand is simultaneously sheared in several orthogonal directions (theoretically six such directions are possible) the resulting settlement is the sum of the settlements which would result from an IP cyclic shearing in the individual directions.

Ishihara & Yamazaki [11] performed undrained simple shear tests with a stress-controlled shearing in two mutually perpendicular directions. Elliptic stress paths were generated (Fig. 6). The amplitude τ_1^{ampl} was kept constant while the amplitude in the orthogonal direction was varied in the range $0 \le \tau_2^{\mathrm{ampl}} \le \tau_1^{\mathrm{ampl}}$. With increasing ratio $\tau_2^{\mathrm{ampl}}/\tau_1^{\mathrm{ampl}}$, i.e. with increasing ovality of the stress loop, the excess pore water pressure accumulation was accelerated and liquefaction was reached earlier (Fig. 6).

The studies in the literature dealing with the influence of the shape and the polarization of the

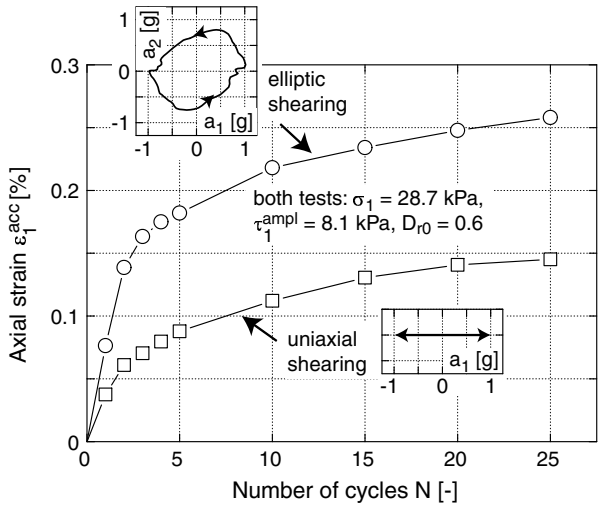

Fig. 5: Shaking table tests after Pyke et al. [10]: comparison of uniaxial and circular stress cycles

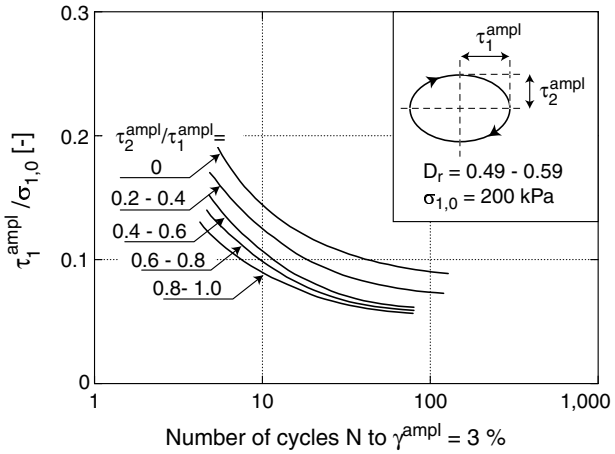

Fig. 6: Undrained simple shear tests after Ishihara & Yamazaki [11]: Influence of the shape (openness) of the stress loop on the liquefaction resistance

stress/strain loop on strain/stress accumulation do not exceed $N \approx 100$. High-quality drained cyclic tests with a larger number of cycles ($N \ge 10^4$) are not known to the authors. Since these tests are indispensable for the development of an explicit accumulation model, they were performed in the framework of the present study.

4 Accumulation model

Our explicit accumulation model is explained in detail in [3]. The main constitutive equation is

$$\dot{\boldsymbol{\sigma}} = \mathsf{E} : (\dot{\boldsymbol{\varepsilon}} - \dot{\boldsymbol{\varepsilon}}^{\mathrm{acc}} - \dot{\boldsymbol{\varepsilon}}^{\mathrm{pl}}) \tag{9}$$

with the stress rate $\dot{\boldsymbol{\sigma}}$, the pressure-dependent elastic stiffness E, the strain rate $\dot{\boldsymbol{\varepsilon}}$, the accumulation rate $\dot{\boldsymbol{\varepsilon}}^{\mathrm{acc}}$ and the plastic strain rate $\dot{\boldsymbol{\varepsilon}}^{\mathrm{pl}}$ (for stress paths touching

the yield surface). The accumulation rate is

$$\dot{\boldsymbol{\varepsilon}}^{\mathrm{acc}} \;=\; \dot{\varepsilon}^{\mathrm{acc}}\,\mathbf{m} \;=\; f_{\mathrm{ampl}}\;\dot{f}_N\;f_e\;f_p\;f_Y\;f_\pi\;\mathbf{m} \quad (10)$$

with the direction of accumulation $\mathbf{m}$ and six scalar functions for the intensity of accumulation, which describe the influences of the strain amplitude (f_{ampl}), the cyclic preloading ($\dot{f}_N$), the void ratio (f_e), the average mean pressure (f_p), the average stress ratio (f_Y) and polarization changes (f_π). For analysing the test results, in this paper we use the amplitude function

$$f_{\mathrm{ampl}} \;=\; (\varepsilon^{\mathrm{ampl}}/\varepsilon^{\mathrm{ampl}}_{\mathrm{ref}})^2 \quad (11)$$

with the reference strain amplitude $\varepsilon^{\mathrm{ampl}}_{\mathrm{ref}} = 10^{-4}$ and the void ratio function

$$f_e \;=\; \frac{(C_e-e)^2}{1+e}\;\frac{1+e_{\mathrm{ref}}}{(C_e-e_{\mathrm{ref}})^2} \quad (12)$$

with the material constant $C_e = 0.54$ and a reference void ratio $e_{\mathrm{ref}} = 0.874$. In order to describe out-of-phase loops we use a multiaxial amplitude definition [2, 3]. From an implicit FE calculation, the strain loop is given as a series of discrete strain points (Fig. 7). First, the two points with maximum distance ($2R_2$) are determined. After that the strain loop is projected in the corresponding direction and the span of the projected loop ($2R_1$) is calculated. The scalar strain amplitude is

$$\varepsilon^{\mathrm{ampl}} \;=\; \sqrt{(R_2)^2+(R_1)^2}. \quad (13)$$

In general, the procedure defines a tensorial amplitude [2, 3].

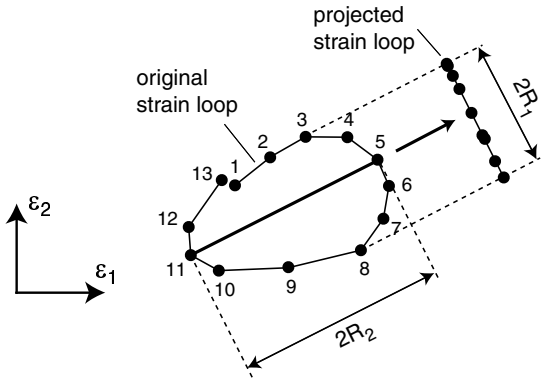

Fig. 7: Determination of the input for the multiaxial amplitude definition, Eq. (13), demonstrated for the two-dimensional case

5 Test device, testing procedure and tested material

5.1 Cyclic triaxial tests

A scheme of the used triaxial cell as well as a detailed description of this test device is given in [4, 6]. Specimens were prepared by pluviating dry sand out of a funnel through air into split moulds. Afterwards the specimens were saturated with de-aired water. A back pressure of 200 kPa was used in all tests. In order to minimize friction the end plates were lubricated and a thin latex membrane was applied. In the analysis of the tests the deformation of this membrane (bedding error) was carefully subtracted from the deformation of the soil skeleton.

The axial load was applied by a pneumatic loading system and was measured inside the pressure cell. The cell pressure σ_3 was varied using a pneumatic pressure valve. The axial deformation of the specimen was measured by means of a displacement transducer which was attached to the load piston. The volume changes were determined via the pore water. Membrane penetration effects are discussed below. During cyclic loading the signals from all transducers were recorded by means of a data acquisition system. In order to reduce the amount of data five complete cycles were sampled in certain intervals. The distance between these recordings was increased logarithmically with the number of cycles N.

Each specimen was consolidated for one hour under the average effective stress $\boldsymbol{\sigma}^{\mathrm{av}}$. After this resting period σ_1 and σ_3 were cyclically varied. Since an air cushion remained in the upper part of the triaxial cell and σ_3 was applied via this air cushion, a sufficiently small loading frequency $f_B = 0.05$ Hz had to be chosen in order to guarantee a sinusoidal course of $\sigma_3(t)$.

Since the lateral effective stress σ_3 was varied, the volume change measured via the pore water contains an additional portion ΔV^{MP} caused by membrane penetration. For an increase of the effective lateral stress from σ_3^A to σ_3^B this portion can be determined from the empirical formula:

$$\Delta V^{\mathrm{MP}} \;=\; \delta V_{\mathrm{MP}}\;A_M \;=\; S\;\log(\sigma_3^B/\sigma_3^A)\;A_M \quad (14)$$

A_M is the area of the membrane being in contact with the specimen, δV_{MP} is the membrane penetration per unit area and S is an empirical factor. In our analysis the formula by Nicholson et al. [12] was used. It correlates S with the grain diameter d_{20}:

$$S \;=\; 0.0019 + 0.0095\;d_{20} - 0.0000157\;(d_{20})^2 \quad (15)$$

with S in the unit [cm^3/cm^2] and d_{20} in [mm]. In our case $d_{20} = 0.4$ mm results in $S = 0.0057$ cm^3/cm^2. The residual volumetric strain $\varepsilon_v^{\mathrm{acc}}$ is not influenced by membrane penetration but the amplitude of volumetric strain $\varepsilon_v^{\mathrm{ampl}}$ has to be corrected.

5.2 Cyclic multidimensional simple shear tests

A scheme of the Cyclic MultiDimensional Simple Shear (CMDSS) device is given in Fig. 8. It is a modification

of the well-known NGI-type (Kjellman [13], Bjerrum und Landva [14]) simple shear device (DSS). The specimen base plate is guided by ball bearings in such way, that only horizontal movements (in both directions x_1 and x_2) are allowed and vertical ones are prevented. The cyclic movement of this plate is caused by an electric motor which rotates an eccentric rod. The eccentric rod transfers only a part of its movement to the base plate depending on the shape of the cut-out in the plate in which the eccentric rod is moving. Different displacement paths in the x_1-x_2-plane (uniaxial and circular paths, different amplitudes) can be tested by using different eccentrics and cut-outs. The top cap can move only in the vertical direction (along x_3), being guided by three ball bearings.

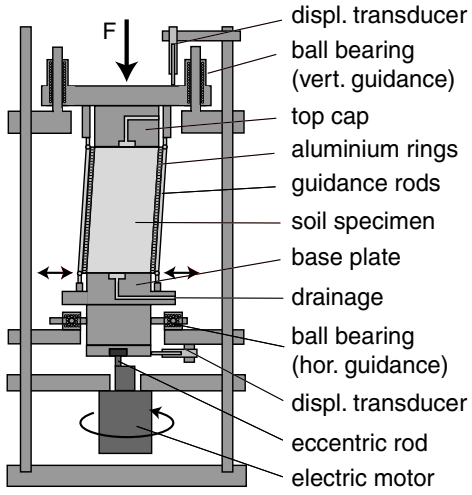

Fig. 8: Scheme of the cyclic multidimensional simple shear (CMDSS) device

Analogously to DSS a lateral deformation of the specimen (diameter $d = 10$ cm, height $h = 20$ cm) is prevented by 200 aluminium rings of 1 mm thickness each. Sand and aluminium rings are separated by a rubber membrane. The aluminum rings are guided by eight extendable vertical rods. They guarantee that the lateral displacements of the rings decrease linearly with the specimen height. This is not necessarily the case in DSS devices. The axial stress σ_1 was applied by placing weights on the upper specimen end plate. Thus, the tests were performed at relatively small stresses. The tests start from an initial K_0 stress. The specimens were prepared by pluviating dry sand out of a funnel. They were also tested in the dry condition. All CMDSS tests were performed with a loading frequency $f_B = 0.5$ Hz. The axial deformation was measured with a displacement transducer. Since no lateral strain is allowed, $\varepsilon^{\mathrm{acc}} = \varepsilon_v^{\mathrm{acc}} = \varepsilon_1^{\mathrm{acc}}$ holds. The horizontal movement of the specimen base plate was controlled by two displacement transducers placed orthogonally to each other. The signals of all transducers were recorded with a data acquisition system.

A simple shear device cannot guarantee a homogeneous distribution of strain over the specimen volume (even when the displacements of the boundaries increase linearly with height, see also Budhu [15, 16]). A study of these inhomogeneities with digital image correlation analysis (DIC) and respective FE calculations [6] revealed larger strain amplitudes at the ends of the specimen compared to its middle. Due to the inhomogeneous strain field, in contrary to the triaxial test the simple shear test cannot be seen as an element test. Therefore, the test results are of a rather qualitative nature. However, the influence of the shape of the strain loop and the effect of polarization changes can be demonstrated clearly by means of this test device.

5.3 Tested material

All tests were performed on a quartz sand with subangular grain shape ($d_{50} = 0.55$ mm, $U = d_{60}/d_{10} = 1.8$, $e_{\max} = 0.874$, $e_{\min} = 0.577$). Its grain size distribution curve was shown as curve No. 1 in Fig. 4 in [4].

6 Influence of the polarization of in-phase cycles

The influence of the polarization of in-phase stress cycles on the accumulation rate was studied in 28 cyclic triaxial tests with a simultaneous oscillation of σ_1 and σ_3. At an average stress with $p^{\mathrm{av}} = 200$ kPa and $\eta^{\mathrm{av}} = 0.5$ different polarization angles $0° \le \alpha_{PQ} \le 90°$ with $\tan(\alpha_{PQ}) = Q^{\mathrm{ampl}}/P^{\mathrm{ampl}}$ were tested. The polarization angle $\alpha_{PQ} = 54.7°$ corresponds to $\sigma_3 =$ constant. For each α_{PQ} four or five tests were performed with stress amplitudes 20 kPa $\le \sqrt{(P^{\mathrm{ampl}})^2 + (Q^{\mathrm{ampl}})^2} \le$ 100 kPa. In Fig. 9a the stress paths are shown in the P-Q-plane.

Fig. 9b presents the resulting strain amplitudes. Independently of the polarization angle α_{PQ}, the strain amplitude $\varepsilon^{\mathrm{ampl}}$ has been observed to be linearly proportional to the stress amplitude (in agreement with linear elasticity). For stress cycles parallel to the P-axis one obtains almost pure volumetric strain cycles. The strain cycles are almost pure deviatoric for stress cycles parallel to the Q-axis. The strain amplitude $\varepsilon^{\mathrm{ampl}}$ increases, i.e. the secant stiffness of the stress-strain-hysteresis decreases, with increasing α_{PQ}. For identical values of the stress amplitude the strain amplitude $\varepsilon^{\mathrm{ampl}}$ due to deviatoric stress cycles ($P^{\mathrm{ampl}} = 0$) is approximately twice larger than that of isotropic stress cycles ($Q^{\mathrm{ampl}} = 0$). Using the elastic relations $P^{\mathrm{ampl}} = 3K\varepsilon_P^{\mathrm{ampl}}$ and $Q^{\mathrm{ampl}} = 2G\varepsilon_Q^{\mathrm{ampl}}$ with bulk modulus K and shear modulus G, one obtains $\varepsilon_Q^{\mathrm{ampl}}/\varepsilon_P^{\mathrm{ampl}} = 3K/2G = (1+\nu)/(1-2\nu)$ for

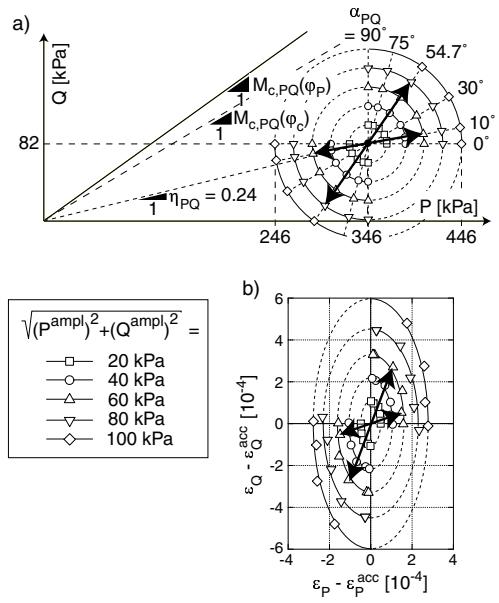

Fig. 9: a) Stress cycles in the P-Q-plane and b) resulting strain amplitudes in the ε_P-ε_Q-plane

$P^{\mathrm{ampl}} = Q^{\mathrm{ampl}}$. The observed factor 2 corresponds to $\nu = 0.2$ (for $\nu = 0$ one would obtain $\varepsilon_Q^{\mathrm{ampl}}/\varepsilon_P^{\mathrm{ampl}} = 1$).

In Fig. 10 the resulting strain loops are summarized for $N = 100$. It is interesting that even perfectly in-phase stress cycles result in oval strain loops due to variable dilatancy.

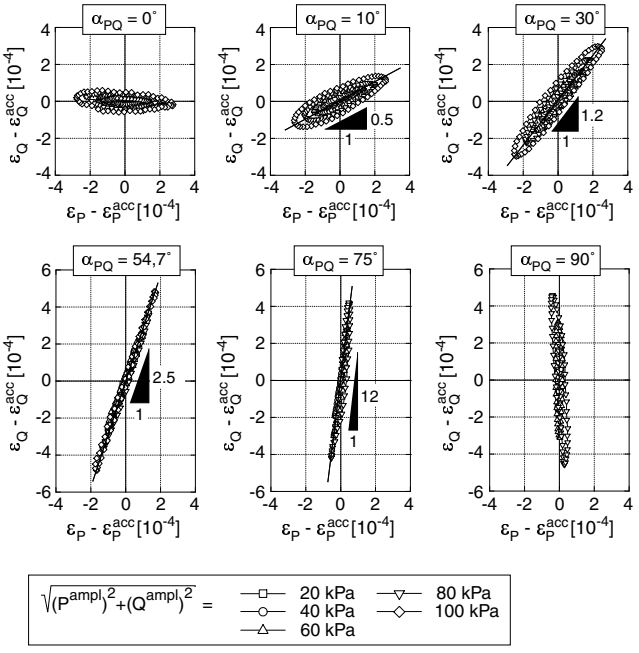

Fig. 10: ε_Q-ε_P-strain loops for stress cycles with different polarization angles α_{PQ} in the P-Q-plane ($N = 100$)

The accumulation curves $\varepsilon^{\mathrm{acc}}(N)$ in the 28 tests are illustrated in Fig. 11. Independently of the polarization angle α_{PQ} the residual strain grows almost linearly with the logarithm of the number of cycles. Thus, test results in [4] for σ_3 = constant were confirmed also for other polarizations.

In Fig. 12 the residual strain after 10^4 cycles is plotted versus the stress amplitude. In order to consider slightly different initial void ratios e_0 and different compaction rates $\dot{e} = \partial e/\partial N$, the accumulated strain $\varepsilon^{\mathrm{acc}}$ was normalized by the void ratio function f_e in Eq. (12). Since e evolves during a test, a mean value $\bar{e}$ of the void ratio in the interval $0 \leftrightarrow N$ was used. The corresponding value of the void ratio function is denoted by $\bar{f}_e$. Figure 12 reveals, that for identical *stress* amplitudes the accumulation rate increases with an increasing deviatoric portion of the stress loop. It is so because $\varepsilon^{\mathrm{ampl}}$ increases with α_{PQ}.

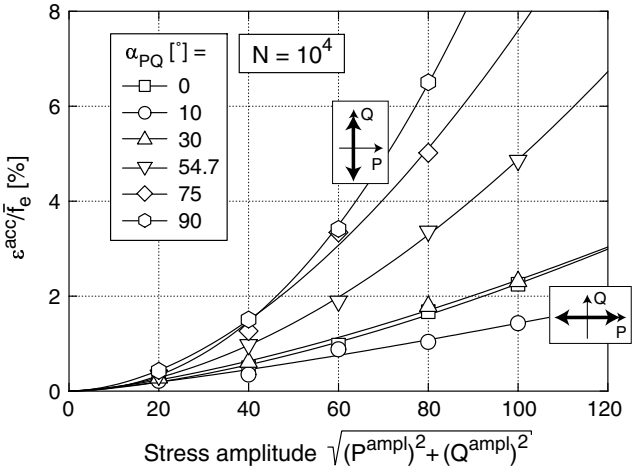

Fig. 12: Accumulated strain $\varepsilon^{\mathrm{acc}}$ at $N = 10^4$ normalized by the void ratio function $\bar{f}_e$ as a function of the stress amplitude for different polarizations α_{PQ}

Most accumulation models (also the one presented in Section 4) are formulated in terms of the *strain* amplitude rather than *stress* amplitude. The advantages of $\boldsymbol{\varepsilon}^{\mathrm{ampl}}$ over $\boldsymbol{\sigma}^{\mathrm{ampl}}$ are discussed in [3]. Figure 13 contains diagrams presenting the residual strain $\varepsilon^{\mathrm{acc}}/\bar{f}_e$ after definite numbers of cycles as a function of $(\bar{\varepsilon}^{\mathrm{ampl}})^2$. The bar over $\bar{\varepsilon}^{\mathrm{ampl}}$ indicates, that (analogously to $\bar{e}$) a mean value of the strain amplitude in the interval $0 \leftrightarrow N$ is used. Each diagram corresponds to a certain polarization angle α_{PQ}. Fig. 13 confirms the relationship $\dot{\varepsilon}^{\mathrm{acc}} \sim (\varepsilon^{\mathrm{ampl}})^2$ (cf. Eq. (11) used in our model) independently of the polarization of the cycles.

In Fig. 14 the residual strain after 10^4 cycles has been normalized by the void ratio function $\bar{f}_e$ and plotted versus the strain amplitude $\bar{\varepsilon}^{\mathrm{ampl}}$. Approximately, the data points for different polarization angles α_{PQ} fall together into a single curve. Thus, for a given *strain* amplitude $\varepsilon^{\mathrm{ampl}}$ the polarization is not significant for the

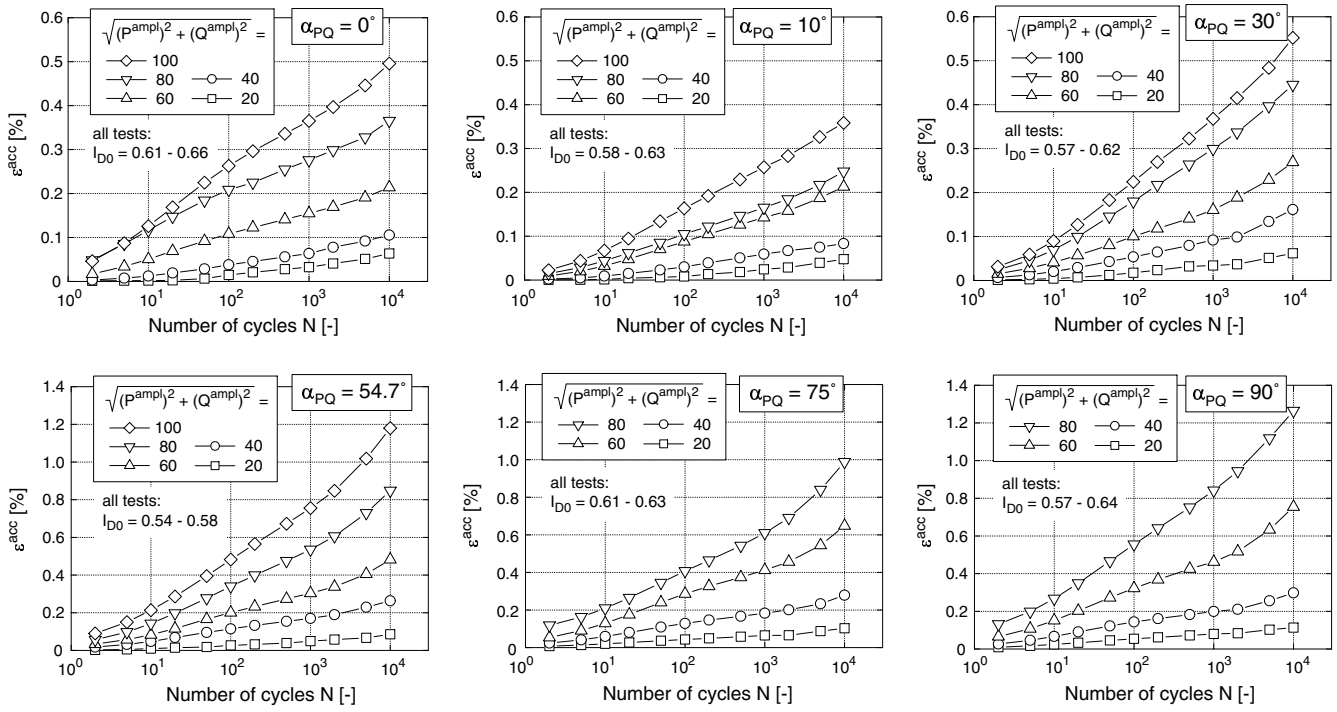

Fig. 11: *Accumulation curves $\varepsilon^{acc}(N)$ for different polarization angles α_{PQ} and stress amplitudes*

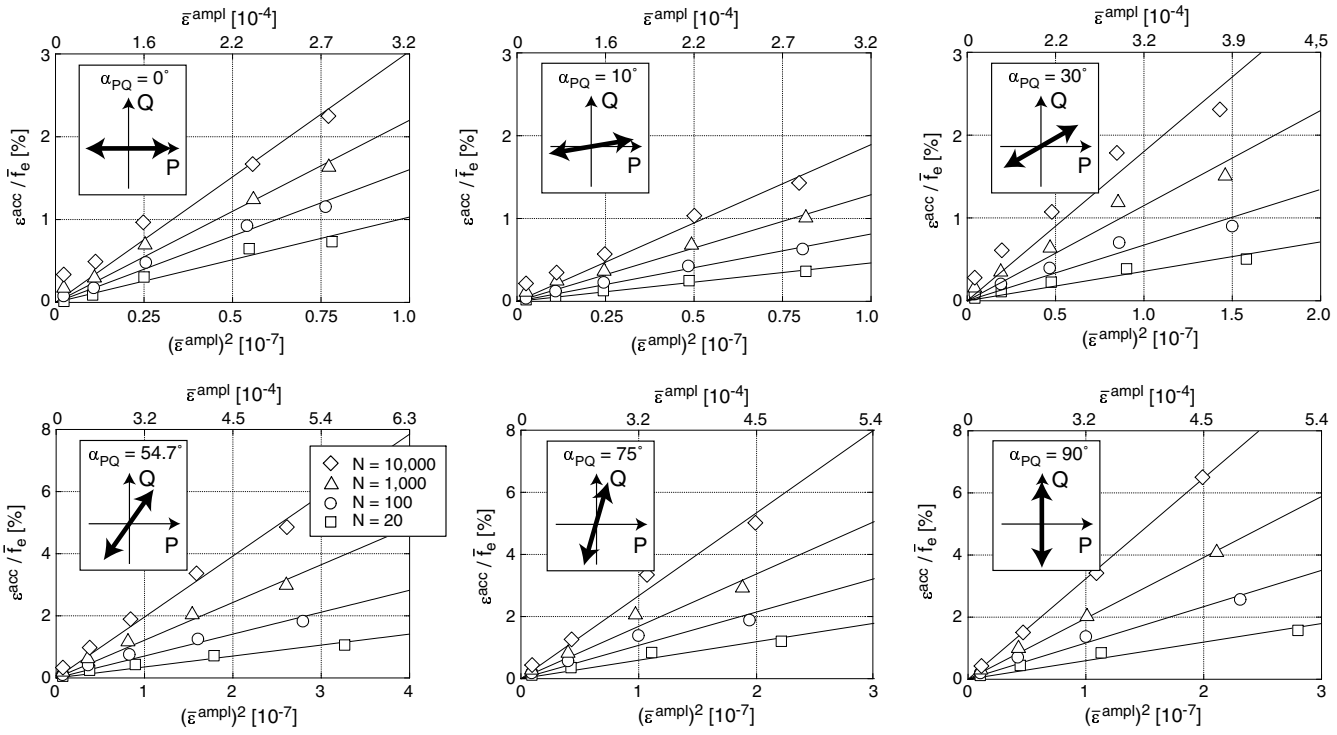

Fig. 13: *Accumulated strain $\varepsilon^{acc}/\bar{f}_e$ as a function of $(\bar{\varepsilon}^{ampl})^2$ for different polarizations α_{PQ} and different numbers of cycles*

accumulation rate, provided it is kept constant. From this test series it can be concluded, that both, the *deviatoric* ($\varepsilon_Q^{\mathrm{ampl}}$) and the volumetric component ($\varepsilon_P^{\mathrm{ampl}}$) of the strain amplitude, contribute equally to the accumulation rate $\dot{\varepsilon}^{\mathrm{acc}}$. Thus, in our model (Section 4) the accumulation rate does not depend on the polarization of the cycles.

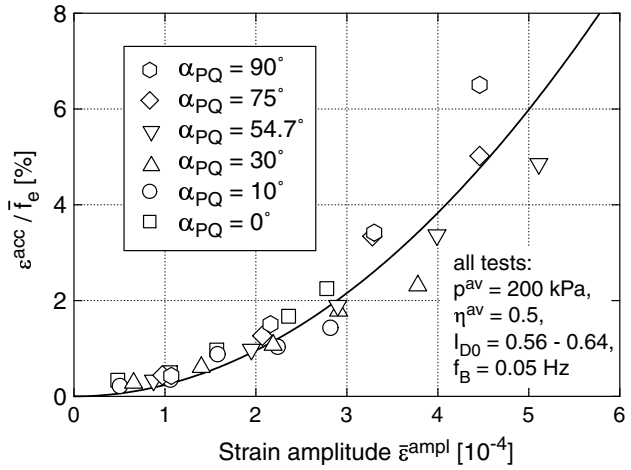

Fig. 14: Accumulated strain $\varepsilon^{\mathrm{acc}}/\bar{f}_e$ after $N = 10^4$ cycles as a function of the strain amplitude $\bar{\varepsilon}^{\mathrm{ampl}}$ for stress cycles with different polarizations α_{PQ} in the P-Q-Ebene

In [4, 5, 17] it was shown, that the direction of accumulation (so-called "cyclic flow rule") $\mathbf{m} = \dot{\boldsymbol{\varepsilon}}^{\mathrm{acc}}/\|\dot{\boldsymbol{\varepsilon}}^{\mathrm{acc}}\|$ is mainly a function of the average stress ratio $\eta^{\mathrm{av}} = q^{\mathrm{av}}/p^{\mathrm{av}}$ and that it does not significantly depend on the average mean pressure p^{av}, the strain amplitude, the void ratio, the loading frequency and the grain size distribution curve. In Fig. 15, for the 28 cyclic triaxial tests with IP cycles, the residual deviatoric strain $\varepsilon_q^{\mathrm{acc}}$ is plotted versus the residual volumetric strain $\varepsilon_v^{\mathrm{acc}}$. Each diagram contains the $\varepsilon_q^{\mathrm{acc}}$-$\varepsilon_v^{\mathrm{acc}}$-paths of the tests with a certain polarization α_{PQ}. For a certain α_{PQ}, the inclination of the $\varepsilon_q^{\mathrm{acc}}$-$\varepsilon_v^{\mathrm{acc}}$ strain paths, i.e. the direction of accumulation $\mathbf{m}$, is only moderately affected by the stress amplitude (although there is some scatter of data for $\alpha_{PQ} = 10°$ and 30°). The six diagrams in Fig. 15 provide an information about the mean value of the inclination $1/\bar{\omega}$. The values lie within $0.97 \leq 1/\bar{\omega} \leq 1.27$. No clear correlation between $1/\bar{\omega}$ and α_{PQ} is noticeable.

7 Influence of polarization changes

7.1 CMDSS tests

A change of the polarization of the cycles causes a temporary increase of the accumulation rate. This is made clear by CMDSS tests with a sudden 90°-change of the direction of cyclic shearing. Figure 16 compares tests with and without a change of the polarization after 1,000 cycles. Different initial densities were tested. The increase of the accumulation rate after a change of the polarization is obvious. This effect of a polarization change decays during the following approx. 1,000 cycles and is independent of the initial density (Fig. 17). In our model the effect of polarization changes is captured by the function f_π (Section 4). Its mathematical formulation is described in [3].

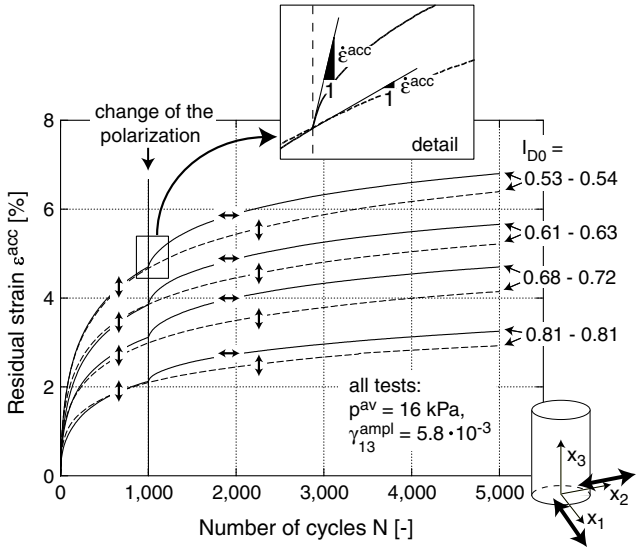

Fig. 16: Temporary increase of the accumulation rate due to a sudden 90°-change of the polarization

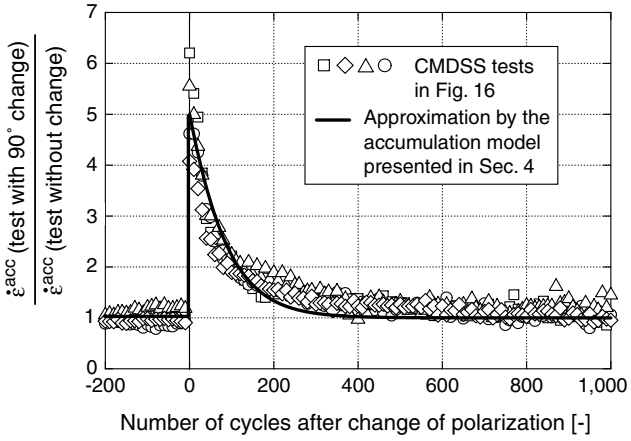

Fig. 17: Decay of the increased accumulation rate during the cycles following the 90°-change of the polarization

7.2 Cyclic triaxial tests

Changes of the polarization could also be studied in cyclic triaxial tests. Two packages of cycles orthogonally polarized in the P-Q-plane were tested. The stress amplitudes were chosen such way that the strain amplitudes were similar for the two polarizations. The accumulation curves of three tests are shown in Fig. 18.

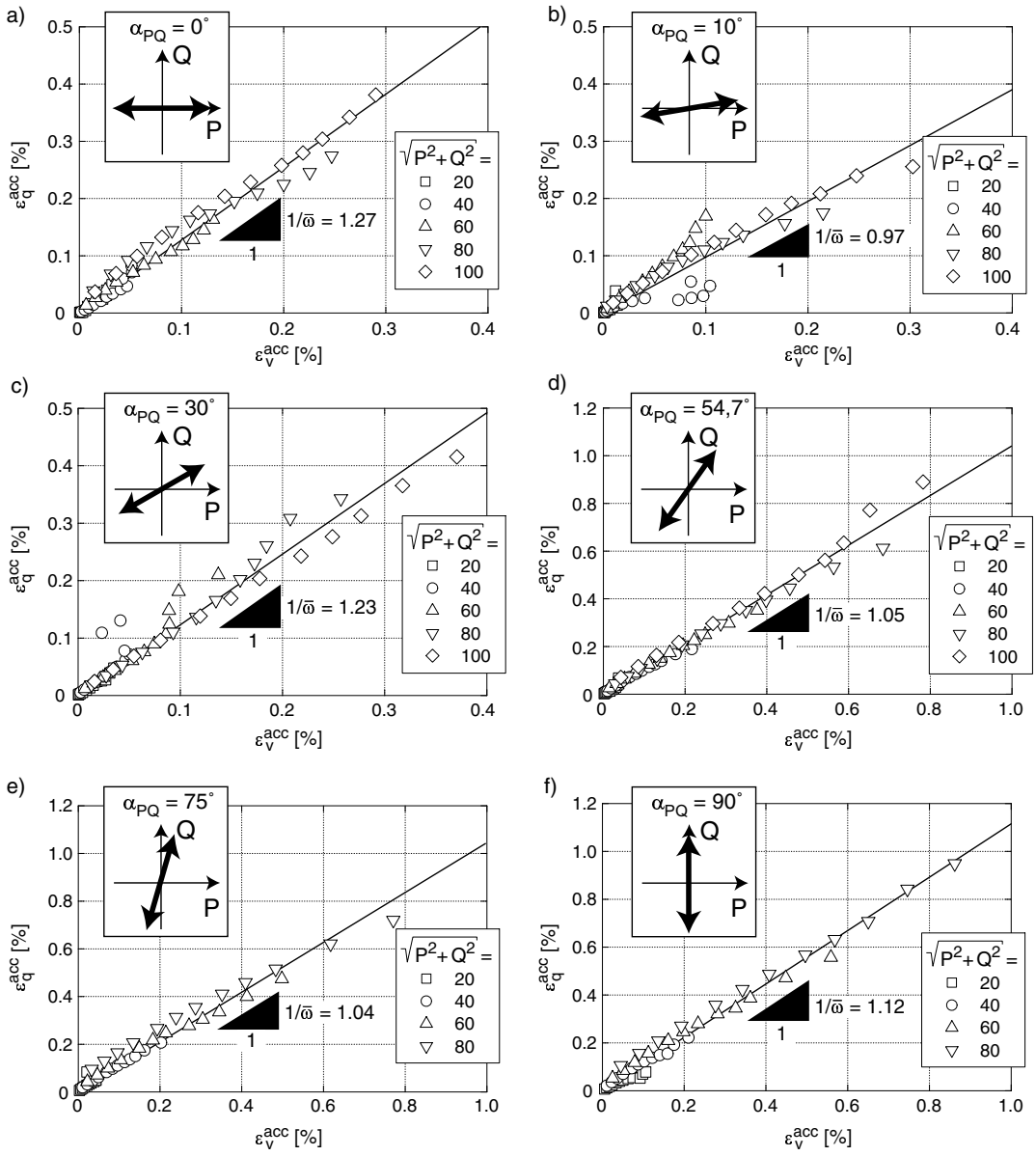

Fig. 15: ε_q^{acc}-ε_v^{acc}-*strain paths for stress cycles with different polarizations in the P-Q-plane (all tests:* $N_{\max} = 10^4$, $p^{av} = 200$ *kPa*, $\eta^{av} = 0.5$, $0.56 \leq I_{D0} \leq 0.64$, $f_B = 0.05$ *Hz)*

The tests Nos. 1 and 2 were performed analogously to the CMDSS tests, i.e. with a single change of the polarization. As in the CMDSS tests a temporary increase of the accumulation rate was observed. In Test No. 3 the polarization was switched (= rotated by 90°) after each cycle. This cyclic loading leads to a much larger residual strain (approx. factor 1.5) than a cyclic loading with the same strain amplitude but a constant polarization.

8 Influence of the shape of the cycles

8.1 CMDSS tests

A circular (OOP) and an uniaxial (IP) cyclic shearing with identical amplitudes in the γ_{13}-direction (Fig. 19) were tested. Figure 19 shows the accumulation curves $\varepsilon^{acc}(N)$ in two tests on initially medium dense specimens during 1,000 cycles. The circular cyclic shearing causes an approximately twice larger accumulation.

Tests with different shear strain amplitudes γ_{13}^{ampl} were performed. In Fig. 20 the accumulated strain after different numbers of cycles is normalized with $\bar{f}_e$ and plotted versus γ_{13}^{ampl}. Figure 20a presents the tests with IP strain cycles while Fig. 20b contains the tests

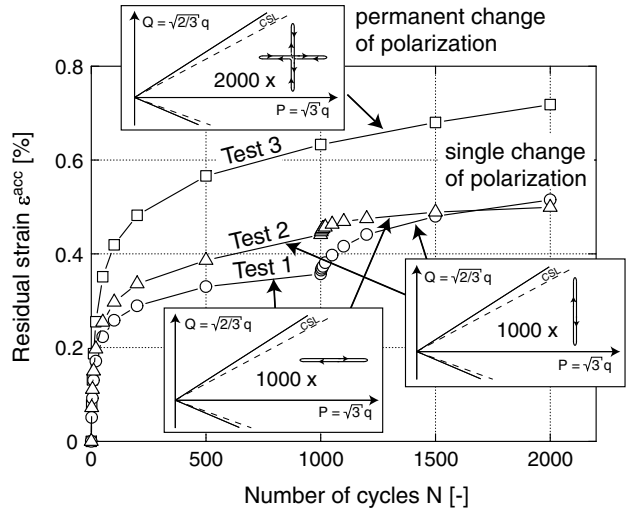

Fig. 18: Cyclic triaxial tests with a single and a permanent change of the direction of the cycles: $P^{\mathrm{av}} = 350$ kPa, $Q^{\mathrm{av}} = 100$ kPa, $P^{\mathrm{ampl}} = 100$ kPa, $Q^{\mathrm{ampl}} = 50$ kPa, $0.56 \leq I_{D0} \leq 0.60$

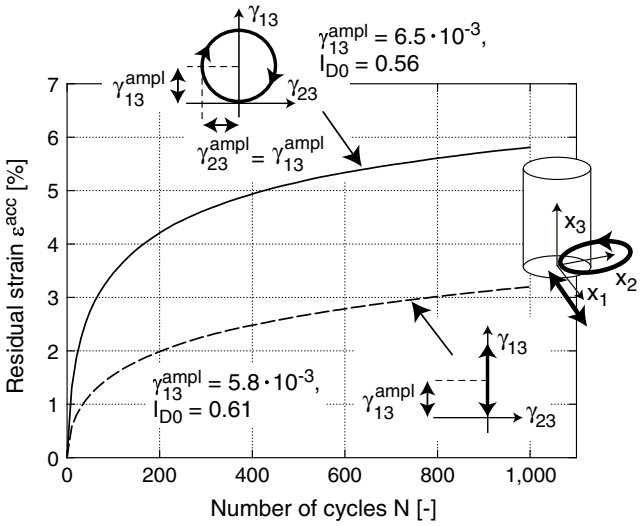

Fig. 19: Comparison of circular and uniaxial (1-D) cycles in CMDSS tests

with circular strain paths ($\gamma_{13}^{\mathrm{ampl}} = \gamma_{23}^{\mathrm{ampl}}$). The difference between the accumulation rates of circular and uniaxial loops increases with N and decreases with $\gamma_{13}^{\mathrm{ampl}}$. The average value of 2 is in good agreement with the tests of Pyke et al. [10] (Fig. 5). The dependence $\dot{\varepsilon}^{\mathrm{acc}} \sim (\gamma_{13}^{\mathrm{ampl}})^2$ was not observed. Possible reasons are the inhomogeneous strain field and the large strain amplitudes. Cyclic triaxial tests [6] revealed that $\dot{\varepsilon}^{\mathrm{acc}} \sim (\varepsilon^{\mathrm{ampl}})^2$ looses its validity for $\varepsilon^{\mathrm{ampl}} > 10^{-3}$. The amplitudes tested in the CMDSS device were all larger than 10^{-3}, for which the proportionality gets lost.

The twice larger accumulation rate for circular loops compared to uniaxial cycles is in accordance with our

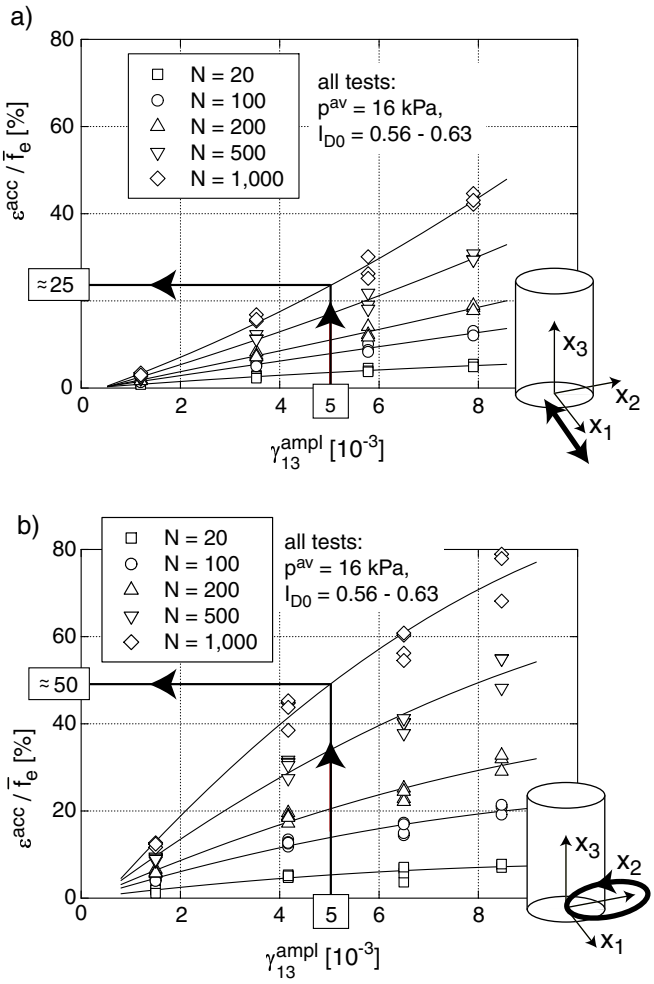

Fig. 20: Comparison of the accumulated strain due to a) uniaxial (1-D) and b) circular strain cycles in the CMDSS device

accumulation model. For uniaxial strain loops with span $2R$ our amplitude definition, Eq. (13), delivers $\varepsilon^{\mathrm{ampl}} = R$. For a circular strain loop with diameter $2R$, Eq. (13) results in $\varepsilon^{\mathrm{ampl}} = \sqrt{2}R$ and considering the amplitude function f_{ampl}, Eq. (11), one obtains indeed the experimentally observed factor 2.

8.2 Cyclic triaxial tests

In the cyclic triaxial tests σ_1 and σ_3 were cyclically varied with a phase shift in time resulting in elliptic stress loops in the P-Q-plane. The cycles were tested on initially medium dense specimens at an average stress with $p^{\mathrm{av}} = 200$ kPa and $\eta^{\mathrm{av}} = 0.5$ (centre of the ellipse in the stress space). The cyclic stress paths in the P-Q-plane are depicted in Fig. 21. The stress paths are well below the critical state line.

The measured stress paths in the P-Q-plane, the resulting ε_P-ε_Q-strain loops as well as the accumulation curves $\varepsilon^{\mathrm{acc}}(N)$ are presented in Fig. 22. Circular

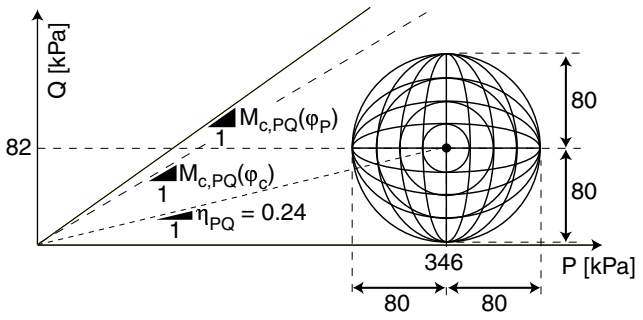

Fig. 21: Elliptic stress paths in the P-Q-plane

P-Q-stress paths lead to slightly inclined elliptic ε_P-ε_Q-strain loops with a considerably longer axis in the ε_Q-direction. With increasing ratio $P^{\mathrm{ampl}}/Q^{\mathrm{ampl}}$ the strain loops become more oval. In the following, referring to Fig. 7, the largest span of the ε_P-ε_Q-ellipse is denoted by $2R_2$ and the smaller one by $2R_1$.

The accumulation curves $\varepsilon^{\mathrm{acc}}(N)$ in the right part of Fig. 22 show that, independently of the shape of the stress/strain loop, the residual strain grows almost linearly proportional to $\ln(N)$. The shape of the curves $\varepsilon^{\mathrm{acc}}(N)$ due to OOP-cycles thus coincides with the curves reported for IP-cycles ([4, **?**] and Fig. 11).

In the test series No. 1 (circular P-Q-stress paths, Fig. 22a) larger strain loops lead to larger accumulation rates. In the series No. 2 (Q^{ampl} = 80 kPa and $P^{\mathrm{ampl}} \leq Q^{\mathrm{ampl}}$, Fig. 22b) due to $\dot{\varepsilon}^{\mathrm{acc}} \sim (\varepsilon^{\mathrm{ampl}})^2$, the small differences in $0.08 \leq R_1/R_2 \leq 0.30$ lead to only moderate differences in the accumulation rates. In the third series (P^{ampl} = 80 kPa and $Q^{\mathrm{ampl}} \leq P^{\mathrm{ampl}}$, Fig. 22c) $\varepsilon_P^{\mathrm{ampl}}$ was almost constant. The ratio of the spans took values $0.3 \leq R_1/R_2 \leq 0.76$. With increasing span of the strain loop in the ε_Q-direction $\dot{\varepsilon}^{\mathrm{acc}}$ increased.

In Fig. 23 the residual strains in the cyclic triaxial tests with OOP- and IP-stress cycles are compared. For the IP-stress cycles $\varepsilon^{\mathrm{ampl}} = R_2$ holds (if one neglects the slight roundness of the corresponding strain loops). In Fig. 23 the residual strain due to the OOP-stress cycles was plotted both versus R_2 (white triangles) and versus $\varepsilon^{\mathrm{ampl}} = \sqrt{(R_2)^2 + (R_1)^2}$ (Eq. (13), gray triangles). The diagram for $N = 10^4$ in Fig. 22 shows the corresponding number of the test. Although the difference between R_2 and $\varepsilon^{\mathrm{ampl}}$ from Eq. (13) is not large (in most tests the ratio R_1/R_2 did not exceed 0.3), $\dot{\varepsilon}^{\mathrm{acc}}$ could be observed to increase with increasing ovality of the strain loops. The accumulation due to 2-D cycles with the spans $2R_2$ and $2R_1$ in the P-Q-space is equivalent to the one of 1-D cycles of the amplitude $\sqrt{(R_2)^2 + (R_1)^2}$ rather than R_2. Using Eq. (13), the accumulation rates of IP- and OOP-cycles can be described by a unique relationship $\dot{\varepsilon}^{\mathrm{acc}} \sim (\varepsilon^{\mathrm{ampl}})^2$ (see the solid curve in Fig. 23), i.e. by the function f_{ampl} of our accumulation model.

Figure 24 presents the $\varepsilon_q^{\mathrm{acc}}$-$\varepsilon_v^{\mathrm{acc}}$-strain paths due to the OOP cycles. A significant dependence of the inclination $1/\bar{\omega}$ of the $\varepsilon_q^{\mathrm{acc}}$-$\varepsilon_v^{\mathrm{acc}}$-strain paths on the shape of the cycles could not be found. Thus, the cyclic flow rule $\mathbf{m}$ is approximately independent of the shape of the cycles.

9 Influence of the circulation

The circulation of the strain loop does not influence the accumulation rate. Figure 25 presents the accumulation curve $\varepsilon^{\mathrm{acc}}(N)$ in a CMDSS test with a change of the circulation from "clockwise" to "counterclockwise" after approx. 500 cycles. No effect of this change on the accumulation rate could be detected.

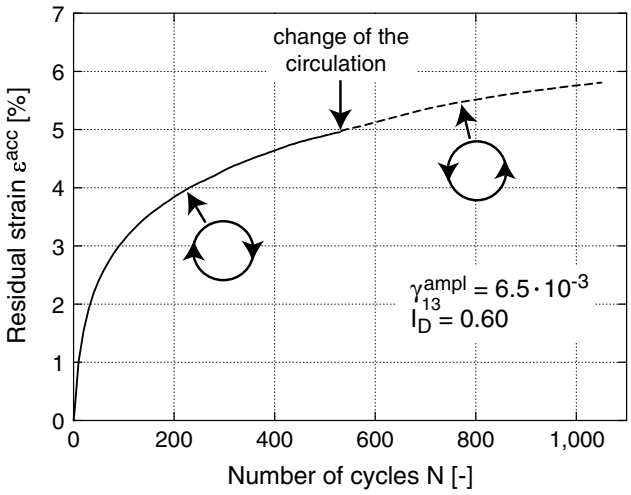

Fig. 25: No influence of a change of the circulaton in a CMDSS test with a circular cyclic shearing

10 Summary and conclusions

The influence of the polarization and the shape of the stress/strain loop on strain accumulation under cyclic loading was studied for a quartz sand with sub-angular grain shape in cyclic triaxial (= CT) tests with a simultaneous oscillation of σ_1 and σ_3. In-phase (IP) and out-of-phase (OOP) cycles were also applied in the cyclic multidimensional simple shear (= CMDSS) apparatus. The results of DSS tests are rather of a qualitative nature and CT tests are much more reliable and of a quantitative nature. Therefore we indicate explicitly the type of test on which the following conclusions were based:

- For a constant size of the *strain* amplitude $\varepsilon^{\mathrm{ampl}}$, the polarization of IP-cycles does not influence the accumulation rate $\dot{\varepsilon}^{\mathrm{acc}}$ (CT)

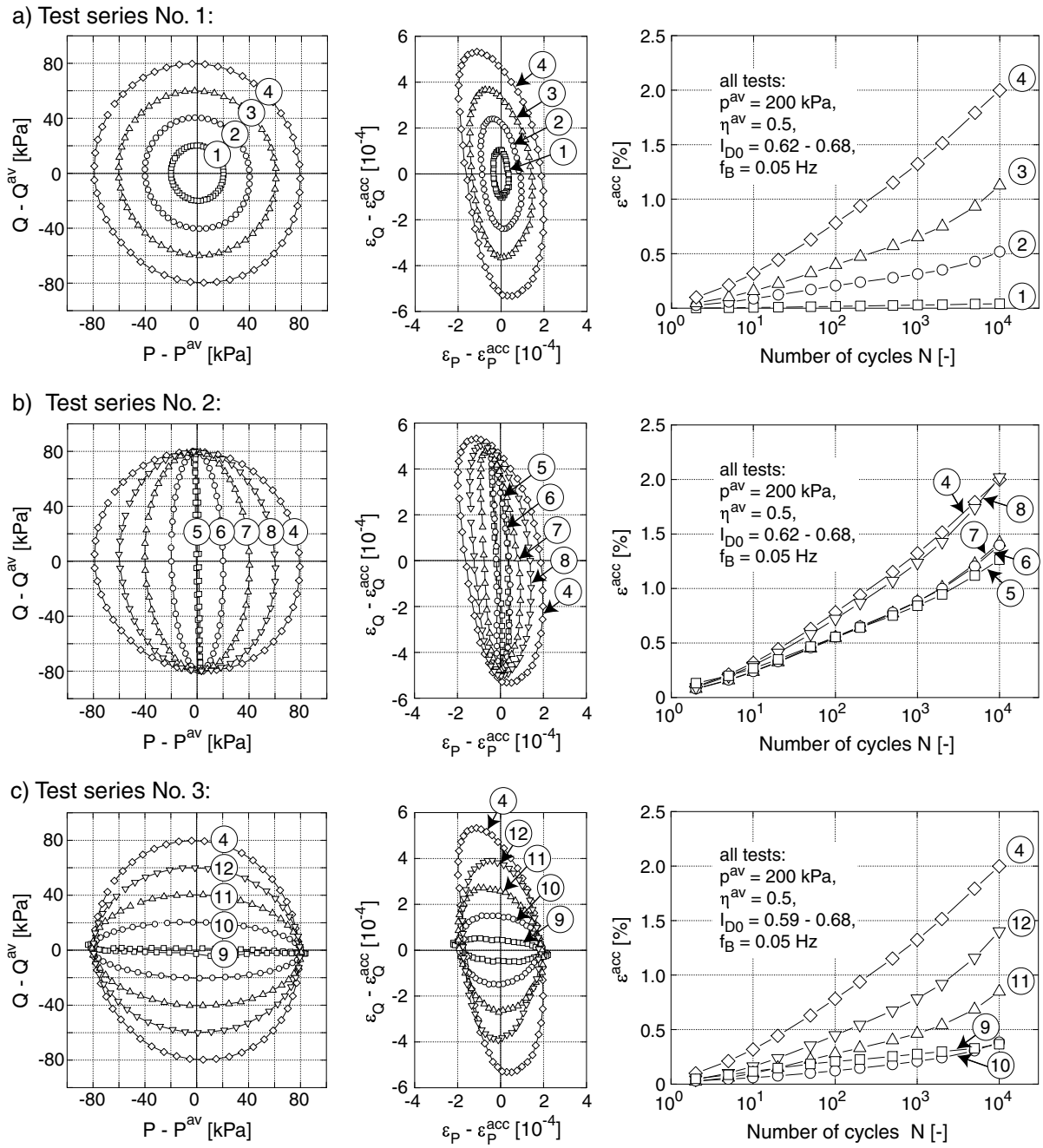

Fig. 22: *P-Q-stress paths, ε_P-ε_Q-strain loops (for N = 1,000) and accumulation curves $\varepsilon^{acc}(N)$ in cyclic triaxial tests with elliptic stress cycles in the P-Q-plane*

- A sudden change of the polarization temporarily increases the accumulation rate (CMDSS, CT). A cyclic loading with a permanent successive change of the polarization leads to approx. 1.5 times larger residual strains than a cyclic loading with a constant polarization (CT)

- The relationship $\dot{\varepsilon}^{\mathrm{acc}} \sim (\varepsilon^{\mathrm{ampl}})^2$ is independent of the polarization of the IP-cycles (at least in the tested range $\varepsilon^{\mathrm{ampl}} \leq 5 \cdot 10^{-4}$) (CT).

- The accumulation curves obeyed $\varepsilon^{\mathrm{acc}} \sim \ln(N)$ for all tested polarizations and shapes of the loop (at least for $N < 10^4$) (CT).

- The direction of accumulation $\mathbf{m} = \dot{\boldsymbol{\varepsilon}}^{\mathrm{acc}} / \|\dot{\boldsymbol{\varepsilon}}^{\mathrm{acc}}\|$ depends neither on the polarization of the IP-cycles, nor on the shape of the stress/strain loop of OOP-cycles (CT).

- OOP-cycles produce larger accumulation rates than IP-cycles if the largest span of the OOP-

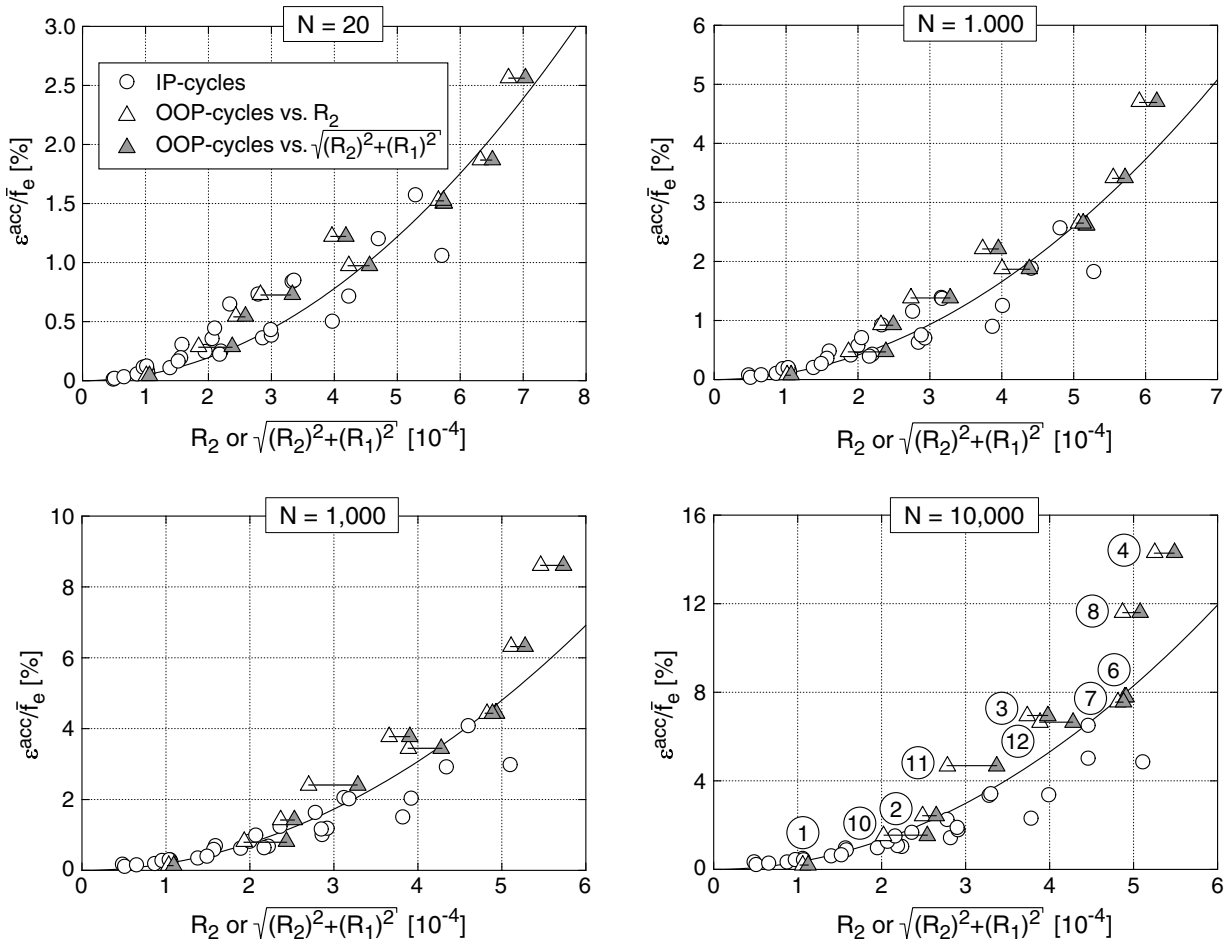

Fig. 23: *Residual strain* $\varepsilon^{acc}/\bar{f}_e$ *as a function of* R_2 *and* $\sqrt{(R_2)^2+(R_1)^2}$*, respectively: comparison of IP- and OOP-cycles*

and the IP-cycles is identical. Circular strain loops generate twice larger accumulation rates than IP strain cycles with identical maximum span (CMDSS).

- The circulation of a strain loop plays no role for $\dot{\varepsilon}^{acc}$ (CMDSS).

Explicit high-cycle accumulation models should consider the shape of the strain loop and the effect of changes of the polarization. The model proposed by the authors (Section 4) with its definition of a multiaxial amplitude [2, 3] obeys these demands. The presented test results corroborate the assumptions of the model.

11 Acknowledgements

This study was conducted as a part of the project A8 "Influence of the fabric change in soil on the lifetime of structures", supported by the German Research Council (DFG) within the Collaborate Research Centre SFB 398 "Lifetime oriented design concepts". The authors are indepted to DFG for this financial support.

References

[1] A. Niemunis. On the estimation of the amplitude of shear strain from measurements in situ. *Soil Dynamics and Earthquake Engineering*, 14:1–3, 1995.

[2] A. Niemunis. Extended hypoplastic models for soils. Habilitation, Veröffentlichungen des Institutes für Grundbau und Bodenmechanik, Ruhr-Universität Bochum, Heft Nr. 34, 2003. available from `www.pg.gda.pl/~aniem/an-liter.html`.

[3] A. Niemunis, T. Wichtmann, and T. Triantafyllidis. A high-cycle accumulation model for sand. *Computers and Geotechnics*, 32(4):245–263, 2005.

[4] T. Wichtmann, A. Niemunis, and T. Triantafyllidis. Strain accumulation in sand due to cyclic loading: drained triaxial tests. *Soil Dynamics and Earthquake Engineering*, 25(12):967–979, 2005.

[5] T. Wichtmann, A. Niemunis, and T. Triantafyllidis. Strain accumulation in sand due to cyclic loading: drained cyclic tests with triaxial exten-

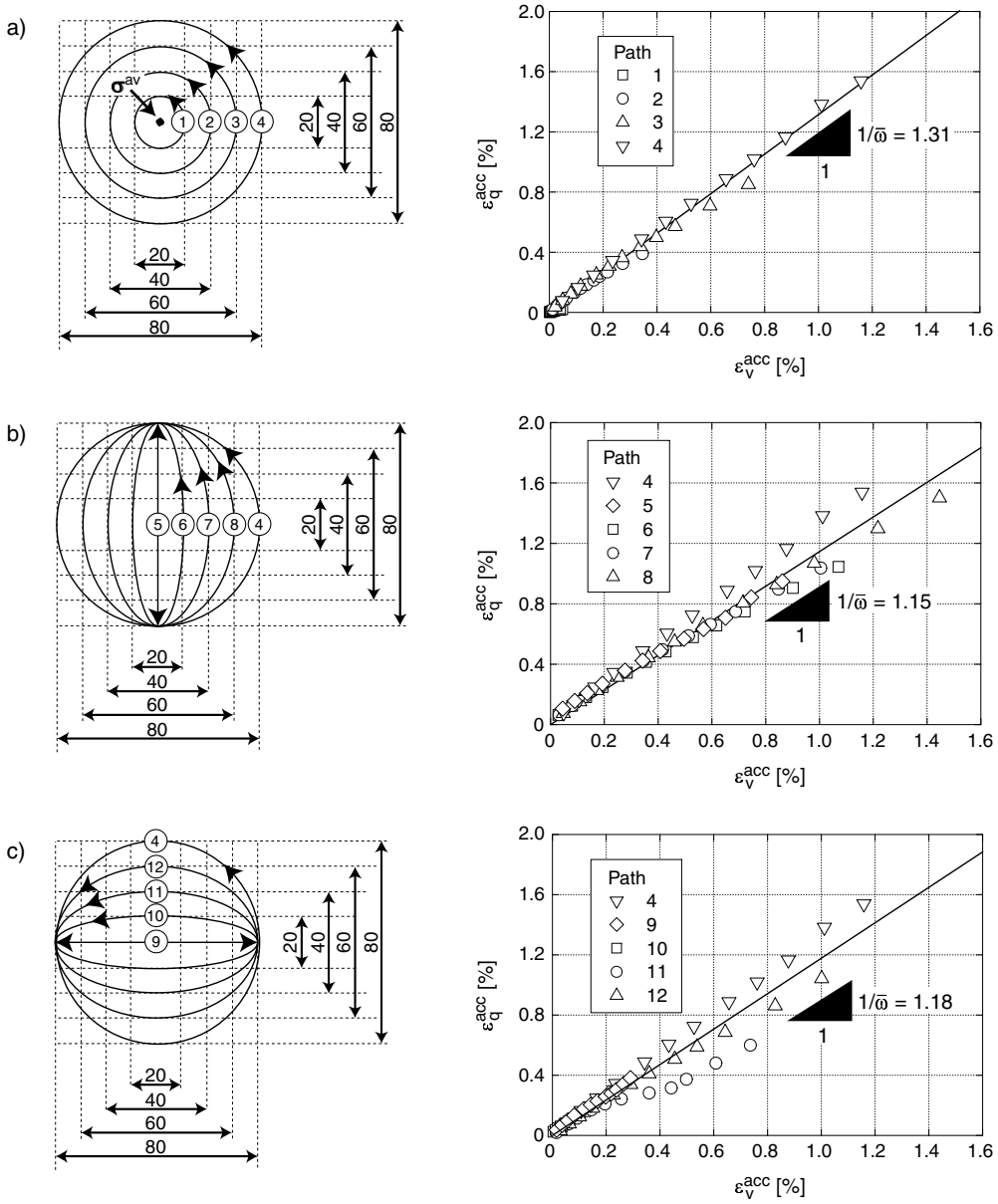

Fig. 24: ε_q^{acc}-ε_v^{acc}-*strain paths for different elliptic stress paths in the P-Q-plane (all tests:* $N_{\max} = 10^4$, p^{av} *= 200 kPa,* η^{av} *= 0.5,* $0.58 \leq I_{D0} \leq 0.68$, f_B *= 0.05 Hz)*

sion. *Soil Dynamics and Earthquake Engineering*, 27(1):42–48, 2007.

[6] T. Wichtmann. Explicit accumulation model for non-cohesive soils under cyclic loading. Dissertation, Schriftenreihe des Institutes für Grundbau und Bodenmechanik der Ruhr-Universität Bochum, Heft 38, available from www.rz.uni-karlsruhe.de/∼gn97/, 2005.

[7] H.Y. Ko and R.F. Scott. Deformation of sand in hydrostatic compression. *Journal of the Soil Mechanics and Foundations Division, ASCE*, 93(SM3):137–156, 1967.

[8] C. Choi and P. Arduino. Behavioral characteristics of gravelly soils under general cyclic loading conditions. In T. Triantafyllidis, editor, *Cyclic behaviour of soils and liquefaction phenomena, Proc. of CBS04*, pages 115–122. Balkema, 2004.

[9] Y. Yamada and K. Ishihara. Yielding of loose sand in three-dimensional stress conditions. *Soils and Foundations*, 22(3):15–31, 1982.

[10] R. Pyke, H.B. Seed, and C.K. Chan. Settlement of sands under multidirectional shaking. *Journal of the Geotechnical Engineering Division, ASCE*, 101(GT4):379–398, 1975.

[11] K. Ishihara and F Yamazaki. Cyclic simple shear tests on saturated sand in multi-directional loading. *Soils and Foundations*, 20(1):45–59, 1980.

[12] P.G. Nicholson, R.B. Seed, and H.A. Anwar. Elimination of membrane compliance in undrained triaxial testing. I. Measurement and evaluation. *Canadian Geotechnical Journal*, 30:727–738, 1993.

[13] W. Kjellman. Testing the shear strength of clay in sweden. *Géotechnique*, 2(3):225–232, 1951.

[14] L. Bjerrum and A. Landva. Direct simple shears tests on a norwegian quick clay. *Géotechnique*, 16(1):2–20, 1966.

[15] M. Budhu. Nonuniformities imposed by simple shear apparatus. *Canadian Geotechnical Journal*, 20:125–137, 1984.

[16] M. Budhu and A. Britto. Numerical analysis of soils in simple shear devices. *Soils and Foundations*, 27(2):31–41, 1987.

[17] T. Wichtmann, A. Niemunis, and T. Triantafyllidis. Experimental evidence of a unique flow rule of non-cohesive soils under high-cyclic loading. *Acta Geotechnica*, 1(1):59–73, 2006.